Journal of Organometallic Chemistry 857 (2018) 88–93

Contents lists available at ScienceDirect

Journal of Organometallic Chemistry

journal homepage: www.elsevier.com/locate/jorganchem

Luminescence differences between two complexes of divalent europium

Brooke A. Corbin [1], Jessica L. Hovey [1], Bishnu Thapa [1], H. Bernhard Schlegel*, Matthew J. Allen**

Department of Chemistry, Wayne State University, 5101 Cass Avenue, Detroit, MI, 48202, United States

ARTICLE INFO

Article history:
Received 11 August 2017
Received in revised form
31 August 2017
Accepted 2 September 2017
Available online 5 September 2017

Keywords:
Cryptate
Divalent europium
Emission
F to d transition
Luminescence
TD-DFT

ABSTRACT

We report a computational study of the photophysical properties of two divalent europium cryptates. Our calculations provide an explanation for the bright yellow luminescence of the Eu^{II}-containing octaaza-cryptate compared to the less intense blue luminescence of the structurally similar Eu^{II}-containing 222-cryptate. Calculations using time-dependent density functional theory with the B3PW91 functional, the Stuttgardt–Dresden relativistic core potential basis for europium, and SMD implicit solvation are used to compute the excitation and emission spectra of both complexes. Emission is also calculated with state-specific solvation. The results are compared with experimental luminescence data acquired in methanol. Natural-transition orbitals reveal similar spin-allowed transitions between the 4f and 5d orbitals on the europium ion in both complexes. For the 222-cryptate, the emissive state is hidden underneath the broad ultraviolet absorption; therefore, the state is not experimentally differentiated in the spectra, despite being present in the calculated spectra. For the octaaza-cryptate, the emissive state is observed as a separate band, shifted to lower energy than the broad ultraviolet absorption. Using ligand-field arguments, sharp differences in luminescence and the bathochromic shift of the emissive state can be attributed to a greater splitting of the 5d orbitals of the octaaza-cryptate relative to the 222-cryptate.

1. Introduction

Divalent lanthanides have been a flourishing area of study, especially with the recent completion of the divalent series by Evans and co-workers [1–22]. Of the divalent lanthanides, europium is of specific interest due to the stability imparted by half-filled 4f orbitals making the divalent state relatively easy to access. Owing to the exceptional electronic stability and distinct magnetic properties, divalent europium has become prevalent in fields such as magnetic resonance imaging [14,19,23–27], photochemistry [28,29], and lanthanide-activated phosphors [16,30,31]. Complexes of divalent europium, like **1** (Fig. 1), generally absorb UV radiation, emit blue light, and have low quantum yields in solution [32] (0.1% quantum yield for **1** in 6:4 methanol/water [33]; ~9.3% quantum yield for **1** in methanol [34]). Recently, we reported a Eu^{II}-containing complex, **2**, that exhibits yellow luminescence with an exceptionally high quantum yield (26% in aqueous solution [13]). The stark difference in luminescence properties between **1** and **2** highlights the need to more thoroughly understand the energetics of **1** and **2** if new Eu-containing luminescent materials are to be designed and studied.

Computational chemistry offers a unique way to investigate the molecular orbitals involved in electronic transitions and predict energies that can be applied to understanding ligand effects. There are few computational studies that report UV–visible spectral models for divalent lanthanide complexes in solution and examine excited states [35–37], and to the best of our knowledge, calculated emission spectra of divalent europium complexes in solution have not been reported. This paucity is likely because a common computational method for lanthanides employs f-in-core pseudopotentials that enforce fixed $4f^n$ configurations [38]. While this enforcement minimizes convergence problems, it precludes studies of f–d luminescence. The lack of reported divalent europium emission studies could also be attributed to the anticipation that Eu^{II} complexes in solution have low quantum yields, similar to **1** [32]. However, given the bright luminescence of **2** and its excitation

* Corresponding author.
** Corresponding author.
E-mail addresses: hbs@chem.wayne.edu (H.B. Schlegel), mallen@chem.wayne.edu (M.J. Allen).
[1] These authors contributed equally.

http://dx.doi.org/10.1016/j.jorganchem.2017.09.007
0022-328X/

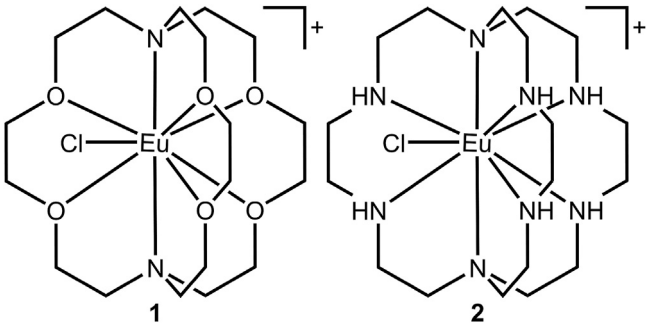

Fig. 1. (left) Eu^{II}-containing 222-cryptate **1** and (right) Eu^{II}-containing octaaza-cryptate **2**.

by visible light, along with other Eu^{II}-containing complexes demonstrating high quantum yields [39–42], the number of interesting systems that contain divalent europium that would benefit from computational analysis is expanding.

In the present study, we used density functional theory to examine the differences in luminescence between **1** and **2**. Our calculations reproduce the expected spin- and dipole-allowed transition from the Eu^{II} ground state ($4f^7$) to the excited state ($4f^65d^1$), and from excited state to ground state [43]. In these transitions, no spin flip is expected due to the strong exchange interaction of Eu^{II} (spin multiplicity = 8). We hypothesized, based on ligand field theory, the difference in electronic energies is likely due to the 5d orbitals that are influenced by the ligand field unlike the shielded 4f orbitals. In our computational study, we compare **1** and **2** because these complexes are structurally similar and have reported absorption, excitation, and emission spectra, with distinct excitation and emission characteristics.

2. Materials and methods

2.1. UV–visible and fluorescence measurements

Commercially available chemicals were of reagent-grade purity or better and were used without further purification unless otherwise noted. Water was purified using a PURELAB Ultra Mk2 water purification system (ELGA). Anhydrous methanol was stored over activated molecular sieves (3 Å) and degassed under reduced pressure (0.2 Torr). The ligand for **1** (4,7,13,16,21,24-hexaoxa-1,10-diazabicyclo[8.8.8]hexacosane) was purchased from TCI chemicals. The ligand for **2** (1,4,7,10,13,16,21,24-octaazabicyclo[8.8.8] hexacosane) was prepared according to a reported procedure [44,45]. Concentrations of Eu were determined using energy-dispersive X-ray fluorescence spectroscopy with an EDX-7000 spectrometer (Shimadzu Scientific Instruments) at the Lumigen Instrument Center at Wayne State University. A calibration curve was used to determine the concentration of a stock solution of $EuCl_2$. The curve was created using the Eu fluorescence intensity at 5.485 keV for a 250–1000 ppm concentration range prepared using a standard solution of europium (Europium Standard for ICP 1002 mg/L Eu in nitric acid, Sigma) and dilutions with water.

Samples of **1** and **2** were complexed in a dry glove box under an atmosphere of N_2 in a 5 mL volumetric flask. Solutions of the complexes were transferred into quartz cuvettes with screw-top caps and sealed with electrical tape to maintain inert atmosphere. UV–visible spectra were recorded using a Shimadzu UVmini-1240 spectrophotometer. Emissions were recorded using a HORIBA Jobin Yvon Fluoromax–4 spectrophotometer. Slit widths of 1 and 0.5 nm were used for excitation and emission, respectively.

2.2. Computational details

All calculations were carried out with the Gaussian 09 suite of programs [46]. Density-functional-theory (DFT) calculations employed the hybrid B3PW91 functional [47–49], the Stuttgardt–Dresden relativistic core potential (SDD) [50,51] basis set for europium, and the D95 basis set for the remaining elements [52]. Calculated structures were tested for self-consistent-field (SCF) stability [53,54]. Solvent effects were modeled using the SMD implicit solvation method [55] in methanol. The ground state geometries of both cryptates were optimized in solution starting from the reported crystal structures [13,26]. The absorption spectra were calculated with time-dependent density functional theory (TD-DFT, 80 states) [56–58]. Spin-orbit effects broaden the 4f–5d transitions of Eu^{II} compounds by 6000 cm^{-1} or more [43] but were not taken into account in the present calculations. For the emission spectra, the lowest energy 4f–5d transition with the highest oscillator strength was chosen for optimization. Fluorescence energies were calculated with state-specific solvation [59,60] and the width of the Gaussian lineshape was adjusted to match experiment. Natural-transition-orbital [61] calculations were used to characterize the excitations. Molecular orbitals and spin densities were plotted with GaussView [62].

3. Results and discussion

To augment the previously reported luminescence data for **1** and **2** [13,33,34], we measured UV–visible and fluorescence spectra with similar concentrations (2–5 mM) in methanol at ambient temperature. Methanol was chosen as the solvent because the reported crystal structures of both **1** and **2** were obtained using crystals grown from methanol, and our calculations used the reported crystal structures as starting coordinates [13,26]. For **1**, our experimental data corresponded well to the reported spectra in methanol [34] and water [33]. We experimentally measured the absorbance maximum for **1** to be 259 nm (38,600 cm^{-1}) and the emission maximum to be 471 nm (21,200 cm^{-1}). For **2**, the reported absorption and emission experiments were run in pH 12 solutions of KOH, and the absorbance maximum was reported as 415 nm (24,100 cm^{-1}) with an emission maximum of 580 nm (17,200 cm^{-1}) [13]. In methanol, we experimentally measured the absorbance maximum for **2** to be 400 nm (25,000 cm^{-1}) and the emission maximum to be 576 nm (17,400 cm^{-1}). Our experimental excitation and emission spectra in methanol differ from aqueous data by 4–15 nm [13], suggesting that computations in methanol serve as good approximations for aqueous photophysical behaviors.

To calculate electronic properties of the divalent-europium-containing cryptates, we started by optimizing the ground-state structures of **1** and **2**. Although structurally comparable, the crystal structures have slightly different geometries: **1** has an eclipsed hula-hoop geometry and **2** has a distorted staggered hula-hoop geometry. Upon optimization with implicit solvation, the structures show good agreement with the reported crystallographic data (Tables S1 and S2 in the Supporting Information). For **1**, the calculated Eu^{II}–O bond lengths range from 2.750 to 2.843 Å compared to the experimental range of 2.659–2.707 Å, and the computed Eu^{II}–N bond lengths range from 2.936 to 3.084 Å compared to the experimental range of 2.838–2.859 Å. The Eu^{II}–Cl bond lengths for **1** computed and measured from crystallographic data are 2.962 and 2.837 Å, respectively. The overall trend for the bonds in **1** shows slightly longer computed bonds compared to crystallographically measured bond lengths, but the differences are in the range reported for the B3PW91 density functional and SDD basis set [63]. A similar lengthening is found for **2**, with the calculated Eu^{II}–N bond lengths ranging from 2.705 to 3.119 Å compared to the

experimental values ranging from 2.675 to 2.958 Å. The calculated Eu^{II}–Cl bond for **2** is 3.286 Å, which is considerably longer than the bond length of 2.694 Å in the crystal structure.

Computational studies of lanthanide luminescence require careful consideration of how spin multiplicity is affected by excitation. For divalent europium in the ground state, the spin multiplicity is eight due to the seven unpaired 4f electrons. Because of strong exchange interactions, the 5d electron in the excited state aligns with the total spin vector, thus simplifying calculations and leaving the spin multiplicity of the system unchanged throughout the original optimization and subsequent calculations. Spin-density plots show that the seven unpaired electrons in the ground states of both **1** and **2** are localized on the metal (Fig. 2).

The broad luminescence curves present in all spectra (Fig. 3) are indicative of a Eu^{II}-containing complex, in part due to spin-orbit effects for the 4f–5d transitions. The TD-DFT calculated absorption spectrum for **1** (broad range of 200–400 nm; maximum absorbance = 277 nm, 36,100 cm^{-1}) reproduced the experimental values (broad range of 230–375 nm; maximum absorbance = 259 nm, 38,600 cm^{-1}). Similarly, the results for **2** are consistent with experiment; the calculated excitation (range of 380–600 nm; maximum absorbance = 427 nm, 23,400 cm^{-1}) are comparable to the experimental values (broad range of 350–550 nm; maximum absorbance = 400 nm, 25,000 cm^{-1}). Both experimental and calculated spectra for **2** showed the same broad higher-energy absorbance curve with the previously reported visible-light excitation curve. Interestingly, the higher-energy curve (experimental maximum absorbance = 269 nm, 37,200 cm^{-1}, calculated maximum absorbance = 260 nm, 38,500 cm^{-1}) is similar in energy to the absorbance curve for **1**.

The excited states in the absorption spectra of **1** and **2** were interpreted by visualizing the natural-transition orbitals. The peak in the absorption spectrum for **1** corresponds to a Laporte-allowed $4f^7$–$4f^65d^1$ excitation. Natural-transition-orbital calculations for this state find that the electronic transition can be described as an excitation from $4f_{z^3}$ orbital to a $5d_{z^2}$ orbital (Fig. 4). For **2**, natural-transition-orbital calculations reveal that the high-energy excited state (260 nm calculated) involves a transition from a $4f_{z^3}$ orbital to a $5d_{z^2}$ orbital. Structure **2** has the distinct visible-light absorbance (400 nm experimental) that initiated interest in the complex. Natural-transition-orbital calculations indicate that this peak corresponds to transition from 4f orbitals to a $5d_{xy}$ orbital. Closer inspection of the calculated absorption spectrum of **1** (Figure S1 in the Supporting Information) reveals a set of weaker excitations than the maximum excitations for **1** forming a shoulder (around 365 nm, 27,400 cm^{-1} calculated) that also involves 4f–$5d_{xy}$ transitions.

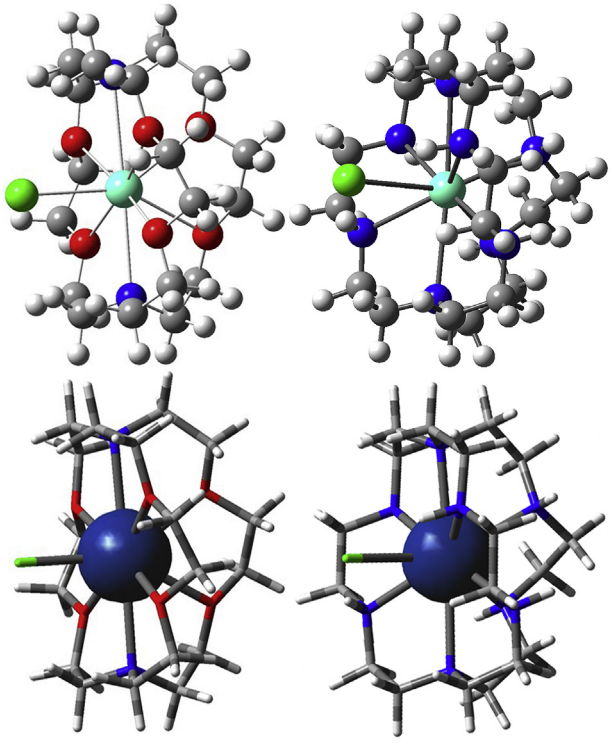

Fig. 2. B3PW91/SDD optimized ground-state structures in SMD methanol: (top left) optimized structure of **1**; (top right) optimized structure of **2**; (bottom left) spin density (blue) mapped onto **1**; (bottom right) spin density (blue) mapped onto **2**.

The changes in the energies of the 4f and 5d orbitals on going from **1** to **2**, and hence the changes in the excitation energies, can be understood qualitatively in terms of ligand field theory. Similar ligand-field arguments have been employed to explain 4f–5d transitions for Ce^{III} [64]. The strong-field character of the N-donors of **2** induces a larger energy splitting (Δ) between the $5d_{z^2}$ and $5d_{xy}$ orbitals compared to the O-donors of **1**, in agreement with the well-established trends of the spectrochemical series (Fig. 5). Consequently, the energy difference between the $5d_{xy}$ and the $4f_{z^3}$ orbitals in **2** is smaller than in **1**; this transition experiences a bathochromic shift in the absorbance spectra with **2** compared to **1**, and this difference in energy moves the transition far enough from the high-energy excitation to appear as a separate peak. While the 4f orbitals are generally shielded from direct interaction with the ligand orbitals, the greater electronegativity of the oxygens in **1** compared to the nitrogen atoms in **2** induces a small (0.40 eV) lowering of the f orbital energies through longer range electrostatic interactions relative to **2**. As a result, the 4f–$5d_{z^2}$ energy difference is nearly the same in the two complexes, and both have strong absorbances near 270 nm.

Emission occurs from the lowest vibrational levels of the lowest $4f^65d^1$ state that has significant oscillator strength for a transition to the ground state (Fig. 4). Geometry optimization of the 4f–$5d_{xy}$ transition of **1** using TD-DFT leads to an average shortening of the Eu^{II}–O and Eu^{II}–N bonds by 0.05 and 0.09 Å, respectively, and a 0.04 Å shortening of the Eu^{II}–Cl bond (Table S1). These changes stabilize the excited state by 1.23 kcal/mol, but the calculated emission maximum at 380 nm (26,300 cm^{-1}) differs considerably from the observed maximum at 471 nm (21,200 cm^{-1}). For **2**, geometry optimization of the emitting state resulted in an average shortening of the Eu^{II}–N bonds by 0.2 Å (Table S2) and a stabilization of the excited state by 11.4 kcal/mol. Interestingly, the bond length of Eu^{II}–Cl extends to the point of full dissociation (4.54 Å), and subsequently the cryptand ligand geometry for **2** changes to become more symmetric, which did not occur for **1**. The emission maximum is calculated to be at 558 nm (17,900 cm^{-1}) and compares well with the observed emission maximum at 576 nm (17,400 cm^{-1}). The good agreement for emission in **2** suggests that there might be another conformer for the lowest excited state of **1** with larger geometric changes and greater stabilization energy that would have a calculated emission peak closer to the experimental value.

In the TD-DFT calculations, solvent effects for the absorption spectra are treated by linear response, which is adequate for states with large transition dipoles [58]. State-specific solvation calculations for the absorption maximum in **1** caused a shift of 11 nm; however, state-specific solvation calculations might be more important for emission because solvation accounts for solvent equilibration for the lowest-energy structure of the emitting state. Considering the state-specific solvation effects on emission, the calculated emission maximum for **1** is shifted to 402 nm, which is a

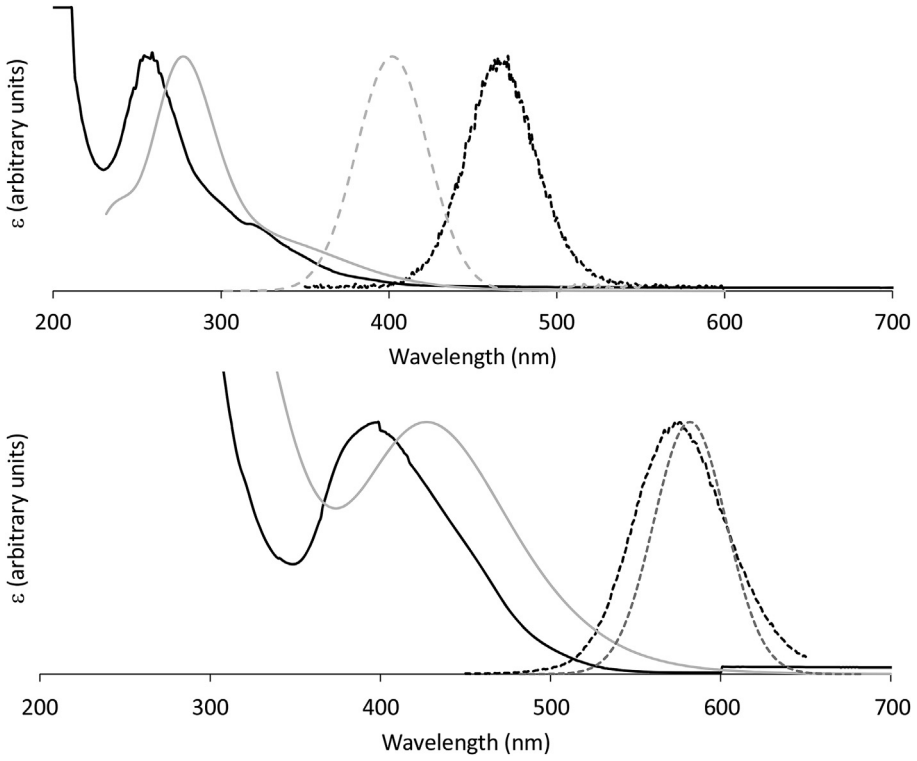

Fig. 3. UV–visible spectra from experiment and TD-DFT B3PW91/SDD calculations in SMD methanol. Experimental absorption (black solid line) and emission (black dashed line) and calculated absorption (grey solid line) and emission (grey dashed line) of **1** (top) and **2** (bottom).

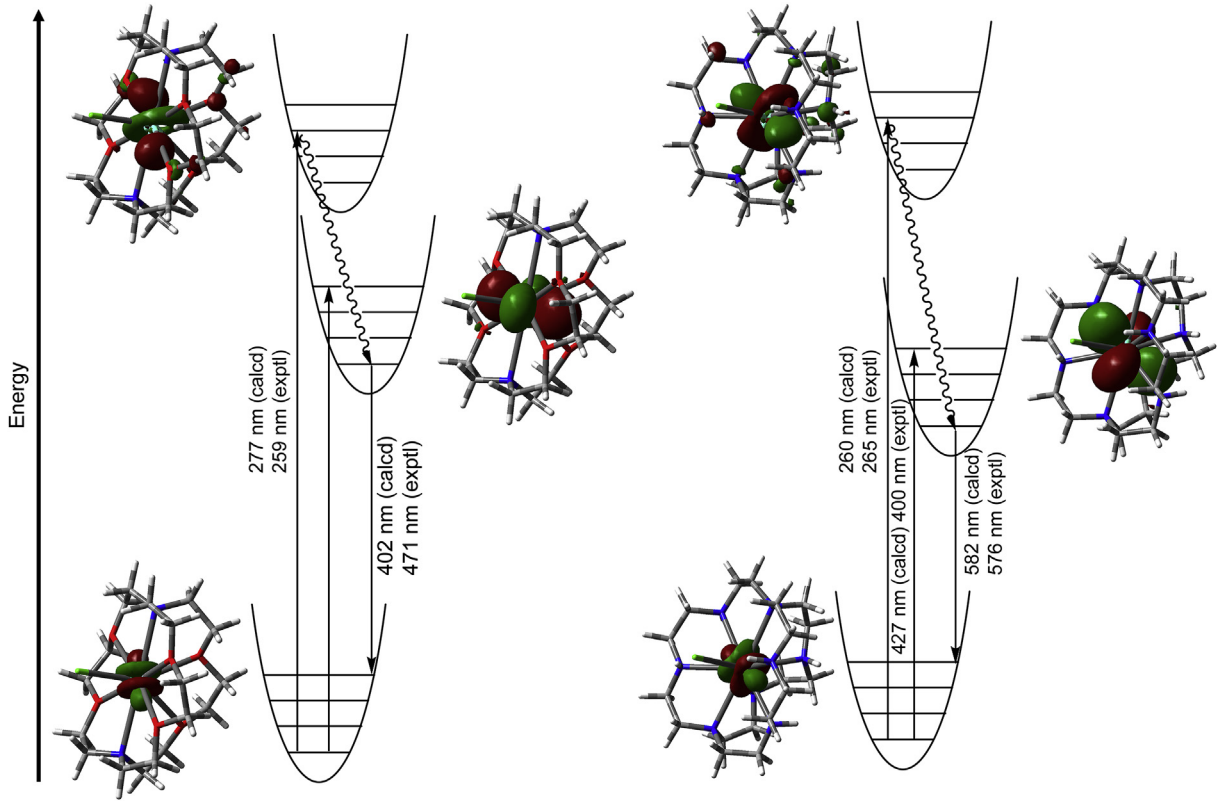

Fig. 4. Energy diagram depicting 4f–5d transitions and the respective natural-transition orbitals involved based on TD-DFT B3PW91/SDD calculations of ground-state-to-excited-state and excited-state-to-ground-state transitions for (left) **1** and (right) **2**.

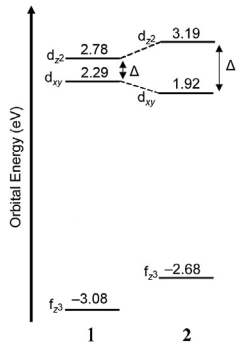

Fig. 5. Orbital energy diagram of the $5d_{z^2}$, $5d_{xy}$, and $4f_{z^3}$ orbitals for **1** (left) and **2** (right). The relatively large splitting energy in **2** is due to the presence of strong-field amine donors in the octaaza-cryptate compared to ethers in **1**.

relatively closer value to the experimental value than the original solvation method. For **2**, the emission maxima with and without state-specific solvation (582 nm and 558 nm) are both in good agreement with the observed value of 576 nm.

The experimental quantum yield for **1** is ~9.3% in methanol, but only 0.1% in water. This difference has been attributed to radiationless deactivation by water [33]. For **2**, the quantum yield in aqueous solution is 26% [13]. Because the absorption and emission involve the same electronic state, there is less opportunity for radiationless deactivation, resulting in a significantly higher quantum yield for **2** than for **1**.

4. Conclusions

We reported the use of TD-DFT calculations as a method to analyze the photophysical properties of divalent-europium-containing complexes. Structurally similar cryptates **1** and **2** were studied because of their different luminescence properties, and the results showed excitation and emission data that reflected experimental data. Natural-transition-orbital calculations provided visualizations of the orbitals of interest in the transition of one electron from the degenerate 4f orbitals to the 5d orbitals. State-specific solvation improved the calculated values for the emission of both **1** and **2**. Based on the strong-field properties of the octaaza-cryptand ligand of **2**, we conclude that the difference in luminescence properties of **1** and **2** are due to a lowering in energy of the emissive state of **2**, resulting in a longer wavelength emission with greater quantum yield than **1**. The present study demonstrates the utility of computational methods in unraveling the complexities of photophysical properties of lanthanide complexes.

Acknowledgements

This work was supported by the National Science Foundation (CHE-1564755 to M.J.A. and CHE-1464450 to H.B.S.). We also thank the Wayne State University computing grid for the computational time.

Appendix A. Supplementary data

Computed Cartesian coordinates (.xyz file); bond lengths and calculated UV−visible spectra (.pdf file).

Supplementary data related to this article can be found at https://doi.org/10.1016/j.jorganchem.2017.09.007.

References

[1] J.D. Rinehart, M. Fang, W.J. Evans, J.R. Long, Nat. Chem. 3 (2011) 538–542.
[2] S. Labouille, F. Nief, X.-F. Le Goff, L. Maron, D.R. Kindra, H.L. Houghton, J.W. Ziller, W.J. Evans, Organometallics 31 (2012) 5196–5203.
[3] M.R. MacDonald, J.E. Bates, J.W. Ziller, F. Furche, W.J. Evans, J. Am. Chem. Soc. 135 (2013) 9857–9868.
[4] L. Soderholm, M.R. Antonio, S. Skanthakumar, C.W. Williams, J. Am. Chem. Soc. 124 (2002) 7290–7291.
[5] C.E. Plečnik, S. Liu, S.G. Shore, Acc. Chem. Res. 36 (2003) 499–508.
[6] G.A. Molander, B. Czakó, D.J. St Jean Jr., J. Org. Chem. 71 (2006) 1172–1180.
[7] L. Raehm, A. Mehndi, C. Wickleder, C. Reyé, R.J.P. Corriu, J. Am. Chem. Soc. 129 (2007) 12636–12637.
[8] K.C. Nicolaou, S.P. Ellery, J.S. Chen, Angew. Chem. Int. Ed. 48 (2009) 7140–7165.
[9] A. Nomoto, Y. Kojo, G. Shiino, Y. Tomisaka, I. Mitani, M. Tatsumi, A. Ogawa, Tetrahedron Lett. 51 (2010) 6580–6583.
[10] C.N. Rao, S. Hoz, J. Org. Chem. 77 (2012) 9199–9204.
[11] P. Starynowicz, Polyhedron 50 (2013) 283–288.
[12] L.A. Ekanger, M.M. Ali, M.J. Allen, Chem. Commun. 50 (2014) 14835–14838.
[13] A.N.W. Kuda-Wedagedara, C. Wang, P.D. Martin, M.J. Allen, J. Am. Chem. Soc. 137 (2015) 4960–4963.
[14] L.A. Ekanger, L.A. Polin, Y. Shen, E.M. Haacke, P.D. Martin, M.J. Allen, Angew. Chem. Int. Ed. 54 (2015) 14398–14401.
[15] P.N. Bartlett, M.J.D. Champion, M.E. Light, W. Levason, G. Reid, P.W. Richardson, Dalton Trans. 44 (2015) 2953–2955.
[16] H. Terraschke, C. Wickleder, Chem. Rev. 115 (2015) 11352–11378.
[17] T.V. Chciuk, W.R. Anderson Jr., R.A. Flowers II, J. Am. Chem. Soc. 138 (2016) 8738–8741.
[18] G.B. Deacon, P.C. Junk, D. Werner, Chem.—Eur. J. 22 (2016) 160–173.
[19] L.A. Basal, Y. Yan, Y. Shen, E.M. Haacke, M. Mehrmohammadi, M.J. Allen, ACS Omega 2 (2017) 800–805.
[20] L.A. Ekanger, L.A. Basal, M.J. Allen, Chem.—Eur. J. 23 (2017) 1145–1150.
[21] S.V. Klementyeva, N.P. Gritsan, M.M. Khusniyarov, A. Witt, A.A. Dmitriev, E.A. Suturina, N.D.D. Hill, T.L. Roemmele, M.T. Gamer, R.T. Boeré, P.W. Roesky, A.V. Zibarev, S.N. Konchenko, Chem.—Eur. J. 23 (2017) 1278–1290.
[22] M. Xémard, A. Jaoul, M. Cordier, F. Molton, O. Cador, B. Le Guennic, C. Duboc, O. Maury, C. Clavaguéra, G. Nocton, Angew. Chem. Int. Ed. 56 (2017) 4266–4271.
[23] É. Tóth, L. Burai, A.E. Merbach, Coord. Chem. Rev. 216–217 (2001) 363–382.
[24] L.A. Ekanger, D.R. Mills, M.M. Ali, L.A. Polin, Y. Shen, E.M. Haacke, M.J. Allen, Inorg. Chem. 55 (2016) 9981–9988.
[25] L.A. Ekanger, L.A. Polin, Y. Shen, E.M. Haacke, M.J. Allen, Contrast Media Mol. Imaging 11 (2016) 299–303.
[26] C.U. Lenora, F. Carniato, Y. Shen, Z. Latif, E.M. Haacke, P.D. Martin, M. Botta, M.J. Allen, Chem.—Eur. J. (2017), http://dx.doi.org/10.1002/chem.201702158.
[27] M. Regueiro-Figueroa, J.L. Barriada, A. Pallier, D. Esteban-Gómez, A. de Blas, T. Rodríguez-Blas, É. Tóth, C. Platas-Iglesias, Inorg. Chem. 54 (2015) 4940–4952.
[28] Y. Tomisaka, A. Nomoto, A. Ogawa, Tetrahedron Lett. 50 (2009) 584–586.
[29] S. Maity, E. Prasad, J. Photochem. Photobiol. A 274 (2014) 64–72.
[30] P. Pust, V. Weiler, C. Hecht, A. Tücks, A.S. Wochnik, A.-K. Henß, D. Wiechert, C. Scheu, P.J. Schmidt, W. Schnick, Nat. Mater 13 (2014) 891–896.
[31] X. Qin, X. Liu, W. Huang, M. Bettinelli, X. Liu, Chem. Rev. 117 (2017) 4488–4527.
[32] J. Jiang, N. Higashiyama, K.-i. Machida, G.-y. Adachi, Coord. Chem. Rev. 170 (1998) 1–29.
[33] N. Sabbatini, M. Ciano, S. Dellonte, A. Bonazzi, F. Bolletta, V. Balzani, J. Phys. Chem. 88 (1984) 1534–1537.
[34] G.-y. Adachi, N. Higashiyama, Nippon. Kagaku Kaishi 5 (1993) 418–432.
[35] M.E. Fieser, M.R. MacDonald, B.T. Krull, J.E. Bates, J.W. Ziller, F. Furche, W.J. Evans, J. Am. Chem. Soc. 137 (2015) 369–382.
[36] M.E. Fieser, C.W. Johnson, J.E. Bates, J.W. Ziller, F. Furche, W.J. Evans, Organometallics 34 (2015) 4387–4393.
[37] J. Christoffers, P. Starynowicz, Polyhedron 27 (2008) 2688–2692.
[38] M. Dolg, H. Stoll, A. Savin, H. Preuss, Theor. Chim. Acta 75 (1989) 173–194.
[39] S. Harder, D. Naglav, C. Ruspic, C. Wickleder, M. Adlung, W. Hermes, M. Eul, R. Pöttgen, D.B. Rego, F. Poineau, K.R. Czerwinski, R.H. Herber, I. Nowik, Chem.—Eur. J. 19 (2013) 12272–12280.
[40] M. Kühling, C. Wickleder, M.J. Ferguson, C.G. Hrib, R. McDonald, M. Suta, L. Hilfert, J. Takats, F.T. Edelmann, New J. Chem. 39 (2015) 7617–7625.
[41] R.P. Kelly, T.D.M. Bell, R.P. Cox, D.P. Daniels, G.B. Deacon, F. Jaroschik, P.C. Junk, X.F. Le Goff, G. Lemercier, A. Martinez, J. Wang, D. Werner, Organometallics 34 (2015) 5624–5636.
[42] C.A.P. Goodwin, N.F. Chilton, L.S. Natrajan, M.-E. Boulon, J.W. Ziller, W.J. Evans, D.P. Mills, Inorg. Chem. 56 (2017) 5959–5970.
[43] P. Dorenbos, J. Phys. Condens. Matter 15 (2003) 575–594.
[44] P.H. Smith, M.E. Barr, J.R. Brainard, D.K. Ford, H. Freiser, S. Muralidharan, S.D. Reilly, R.R. Ryan, L.A. Silks III, W.-h. Yu, J. Org. Chem. 58 (1993) 7939–7941.
[45] M.Y. Redko, R. Huang, J.L. Dye, J.E. Jackson, Synthesis 5 (2006) 759–761.
[46] M.J. Frisch, G.W. Trucks, H.B. Schlegel, G.E. Scuseria, M.A. Robb, J.R. Cheeseman, G. Scalmani, V. Barone, G.A. Petersson, H. Nakatsuji, X. Li, M. Caricato, A.V. Marenich, J. Bloino, B.G. Janesko, R. Gomperts, B. Mennucci,

H.P. Hratchian, J.V. Ortiz, A.F. Izmaylov, J.L. Sonnenberg, D. Williams-Young, F. Ding, F. Lipparini, F. Egidi, J. Goings, B. Peng, A. Petrone, T. Henderson, D. Ranasinghe, V.G. Zakrzewski, J. Gao, N. Rega, G. Zheng, W. Liang, M. Hada, M. Ehara, K. Toyota, R. Fukuda, J. Hasegawa, M. Ishida, T. Nakajima, Y. Honda, O. Kitao, H. Nakai, T. Vreven, K. Throssell, J.A. Montgomery Jr., J.E. Peralta, F. Ogliaro, M.J. Bearpark, J.J. Heyd, E.N. Brothers, K.N. Kudin, V.N. Staroverov, T.A. Keith, R. Kobayashi, J. Normand, K. Raghavachari, A.P. Rendell, J.C. Burant, S.S. Iyengar, J. Tomasi, M. Cossi, J.M. Millam, M. Klene, C. Adamo, R. Cammi, J.W. Ochterski, R.L. Martin, K. Morokuma, O. Farkas, J.B. Foresman, D.J. Fox, Gaussian 09, Revision E.01, Gaussian, Inc., Wallingford CT, 2016.
[47] A.D. Becke, J. Chem. Phys. 98 (1993) 5648–5652.
[48] J.P. Perdew, Phys. Rev. B 33 (1986) 8822–8824.
[49] J.P. Perdew, K. Burke, Y. Wang, Phys. Rev. B 54 (1996) 16533–16539.
[50] X. Cao, M. Dolg, J. Chem. Phys. 115 (2001) 7348–7355.
[51] X. Cao, M. Dolg, J. Mol. Struct. 581 (2002) 139–147.
[52] L.B. Harding, W.A. Goddard III, J. Chem. Phys. 67 (1977) 2377–2379.
[53] R. Seeger, J.A. Pople, J. Chem. Phys. 66 (1977) 3045–3050.
[54] R. Bauernschmitt, R. Ahlrichs, J. Chem. Phys. 104 (1996) 9047–9052.
[55] A.V. Marenich, C.J. Cramer, D.G. Truhlar, J. Phys. Chem. B 113 (2009) 6378–6396.
[56] R.E. Stratmann, G.E. Scuseria, M.J. Frisch, J. Chem. Phys. 109 (1998) 8218–8224.
[57] F. Furche, R. Ahlrichs, J. Chem. Phys. 117 (2002) 7433–7447.
[58] G. Scalmani, M.J. Frisch, B. Mennucci, J. Tomasi, R. Cammi, V. Barone, J. Chem. Phys. 124 (2006) 094107.
[59] R. Improta, V. Barone, G. Scalmani, M.J. Frisch, J. Chem. Phys. 125 (2006) 054103.
[60] R. Improta, G. Scalmani, M. Frisch, V. Barone, J. Chem. Phys. 127 (2007) 74504.
[61] R.L. Martin, J. Chem. Phys. 118 (2003) 4775–4777.
[62] T.K.R. Dennington, J. Milliam, Gaussview, Version 5, Semichem Inc., Shawnee Mission, KS, 2009.
[63] D. Wang, C. Zhao, D.L. Phillips, Organometallics 23 (2004) 1953–1960.
[64] H. Yin, P.J. Carroll, B.C. Manor, J.M. Anna, E.J. Schelter, J. Am. Chem. Soc. 138 (2016) 5984–5993.